RESEARCH ARTICLE

Parametric study of separation and transition characteristics over an airfoil at low Reynolds numbers

Michael S. H. Boutilier · Serhiy Yarusevych

Abstract Time-resolved surface pressure measurements are used to experimentally investigate characteristics of separation and transition over a NACA 0018 airfoil for the relatively wide range of chord Reynolds numbers from 50,000 to 250,000 and angles of attack from 0° to 21°. The results provide a comprehensive data set of characteristic parameters for separated shear layer development and reveal important dependencies of these quantities on flow conditions. Mean surface pressure measurements are used to explore the variation in separation bubble position, edge velocity in the separated shear layer, and lift coefficients with angle of attack and Reynolds number. Consistent with previous studies, the separation bubble is found to move upstream and decrease in length as the Reynolds number and angle of attack increase. Above a certain angle of attack, the proximity of the separation bubble to the location of the suction peak results in a reduced lift slope compared to that observed at lower angles. Simultaneous measurements of the time-varying component of surface pressure at various spatial locations on the model are used to estimate the frequency of shear layer instability, maximum root-mean-square (RMS) surface pressure, spatial amplification rates of RMS surface pressure, and convection speeds of the pressure fluctuations in the separation bubble. A power-law correlation between the shear layer instability frequency and Reynolds number is shown to provide an order of magnitude estimate of the central frequency of disturbance amplification for various airfoil geometries at low Reynolds numbers. Maximum RMS surface pressures are found to agree with values measured in separation bubbles over geometries other than airfoils, when normalized by the dynamic pressure based on edge velocity. Spatial amplification rates in the separation bubble increase with both Reynolds number and angle of attack, causing the accompanying decrease in separation bubble length. Values of the convection speed of pressure fluctuations in the separated shear layer are measured to be between 35 and 50% of the edge velocity, consistent with predictions of linear stability theory for separated shear layers.

List of symbols

C_L Sectional lift coefficient
C_p Mean surface pressure coefficient
c Model chord length
d Model height projected onto a streamwise-normal plane
E_{pp} Normalized energy spectrum of surface pressure fluctuations
f Frequency
f_0 Central frequency of disturbance amplification
L Separation bubble length
n Exponent in experimental correlations
$\tilde{p}$ RMS surface pressure
$\tilde{p}_{max}$ Maximum RMS surface pressure at a particular α
q_e Dynamic pressure based on edge velocity, $q_e = \frac{1}{2}\rho U_e^2$
q_∞ Free-stream dynamic pressure, $q_\infty = \frac{1}{2}\rho U_\infty^2$
Re Chord Reynolds number, $Re = U_\infty c/\nu$
St Strouhal number for central frequency of disturbance amplification, $St = f_0 d/U_\infty$
U_c Convection speed of surface pressure fluctuations in the separation bubble
U_e Mean edge velocity in the separated shear layer
U_∞ Free-stream velocity

M. S. H. Boutilier · S. Yarusevych (✉)
University of Waterloo, 200 University Ave. W.,
Waterloo, ON N2L 3G1, Canada
e-mail: syarus@uwaterloo.ca

$\tilde{u}$ RMS free-stream velocity

x Distance from the leading edge of the airfoil, measured along the chord

α Angle of attack

ν Kinematic viscosity

ρ Fluid density

σ Exponential spatial amplification factor of RMS surface pressure

1 Introduction

Flow development over airfoils operating at low chord Reynolds numbers is of interest for the design of certain engineering systems, including micro air vehicles and small wind turbines. These devices commonly employ airfoils operating in the chord Reynolds number range between 10,000 and 500,000 (Lissaman 1983; Mueller 1985; Mueller and DeLaurier 2003; Carmichael 1981; Bansmer et al. 2010). As sketched in Fig. 1, in this Reynolds number regime, the boundary layer on the upper surface of the airfoil remains laminar into the pressure recovery region, often resulting in boundary layer separation. When the boundary layer separates, transition to turbulence typically occurs in the separated shear layer, leading to turbulent boundary layer reattachment and the formation of a separation bubble at low angles of attack. At higher angles of attack, the turbulent shear layer remains separated. The aerodynamic performance of airfoils at low Reynolds numbers is largely determined by the characteristics of separation and transition (Lissaman 1983; Mueller 1985; Mueller and DeLaurier 2003).

A number of experimental studies have measured aerodynamic forces on airfoil sections operating at low Reynolds numbers (Carmichael 1981; Tani 1964; Marchman 1987; Mueller and Batill 1982; Laitone 1997; Pelletier and Mueller 2000; Gerakopulos et al. 2010). These investigations have provided data for a wide range of flow conditions and airfoil geometries, but are limited in the amount of detail about flow development that can be extracted from the results. Other investigations have focused on characterizing flow development, with particular attention to transition in the separation bubble (O'Meara and Mueller 1987; Brendel and Mueller 1988; Burgmann et al. 2006; Burgmann and Schröder 2008; Zhang et al. 2008; Yarusevych et al. 2009; Hain et al. 2009). Studies on flat plates and airfoils have shown vortex roll-up occurring in the separated shear layer at the frequency of dominant disturbance amplification, with vortex pairing occurring downstream for some flow conditions (Burgmann and Schröder 2008; Zhang et al. 2008; Yarusevych et al. 2009; Hain et al. 2009; Watmuff 1999; Lang et al. 2004). Based on experimental data for a number of airfoils operating at low Reynolds number conditions, Yarusevych et al. (2009) suggested a power-law dependence of the central frequency of disturbance amplification on chord Reynolds number. In a recent study by Burgmann and Schröder (2008), detailed time-resolved measurements of the velocity field over an SD 7003 airfoil were used to identify several types of coherent vortical structures that develop during transition. Burgmann and Schröder (2008) attributed qualitative differences in the coherent structures observed in their experiments from those observed over flat plates by Watmuff (1999) and Lang et al. (2004) to a dependence of transition behavior on surface curvature. A dependence of coherent structure development on flow conditions was also observed. The time required to complete the detailed measurements necessary for such investigations has limited these studies to a small number of flow conditions and airfoil geometries. Measurements of transition characteristics over a wider range of flow conditions and airfoil geometries may reveal further details about the qualitative dependence of the transitioning flow on surface curvature and flow conditions.

Time-resolved surface pressure measurements are a compromise between broad aerodynamic characterizations and detailed measurements of flow development. Surface pressure sensor arrays can be used to measure pressure field

Fig. 1 Time-averaged transitional separation bubble model, after Ellsworth and Mueller (1991)
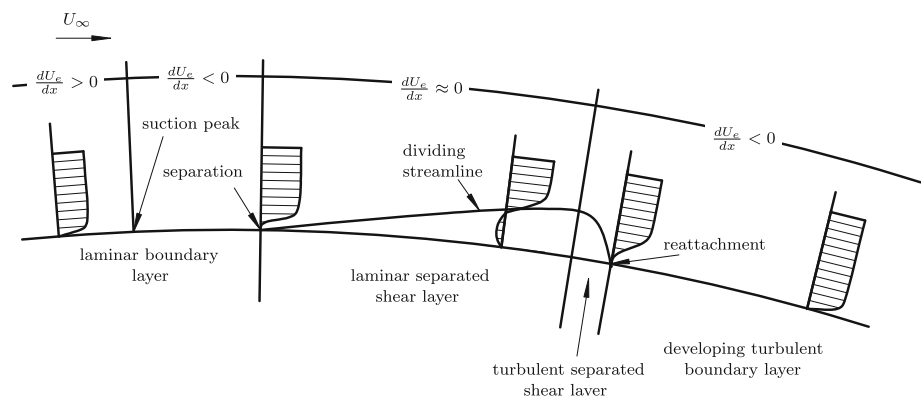
development at multiple spatial locations with a high sampling rate, providing more detailed information than force balance measurements in significantly less time than is required for full flow field mapping. From these data, characteristics of the separated flow region can be determined (Tani 1964; O'Meara and Mueller 1987; Schmidt and Mueller 1989) and disturbance development can be measured (Yarusevych et al. 2008; Gerakopulos and Yarusevych 2012; Boutilier 2011). Such sensors also provide minimal obstruction to the flow and have a sufficiently fast response time that they could be employed in flapping wing experiments, which are relevant to micro air vehicle design (Bansmer et al. 2010). The present investigation focuses on aspects of separation and transition over an airfoil, for a wide range of low Reynolds number conditions, that can be measured using an array of time-resolved surface pressure sensors.

Surface pressure measurements have been used to gain insight into flow development over various geometries. Willmarth (1975) summarizes several investigations that have considered the pressure fluctuations on the surface beneath turbulent boundary layers to identify sources of noise and vibrations on aircraft. Paterson et al. (1973) used arrays of five microphones embedded in the surface of NACA 0012 and NACA 0018 airfoil models to investigate sources of noise generation at chord Reynolds numbers between 400,000 and 3,000,000. They showed that the propagation speed of surface pressure fluctuations could be determined from a cross-correlation of microphone responses. They also showed that the microphone signals could be used to identify whether the boundary layer is laminar or turbulent, based on the relative magnitudes of pressure fluctuations in these regimes. A number of investigations have employed surface pressure sensors to study separation bubble development (Mabey 1972; Hudy et al. 2003; Farabee and Casarella 1986; Driver et al. 1987; Lee and Sung 2001; Cherry et al. 1984; Weibust et al. 1987). Separation bubbles forming over blunt splitter plates, splitter plates with fences, forward facing steps, backward facing steps, and in pipe expansion sections show similar trends (Mabey 1972; Hudy et al. 2003; Farabee and Casarella 1986; Driver et al. 1987; Lee and Sung 2001; Cherry et al. 1984; Weibust et al. 1987); root-mean-square (RMS) pressure fluctuations increase in the separated flow to a maximum just upstream of the mean reattachment point and decay downstream.

Convection speeds on the order of 50–60% of the free-stream velocity in separation bubbles on blunt face splitter plates (Cherry et al. 1984) and backward facing steps (Farabee and Casarella 1986) have been measured by analyzing cross-spectra and cross-correlations of measurements from pairs of embedded pressure sensors. Frequency wave number energy spectrum analysis has been used by Lee and Sung (2001), on the separation bubble behind a backward facing step, and by Hudy et al. (2003), on the separation bubble formed behind a fence on a splitter plate. In both investigations, a ridge in the spectrum corresponding to the downstream convection speed was identified. Hudy et al. (2003) observed a second ridge in the spectrum corresponding to an upstream convection speed of approximately 20% of the free-stream velocity. They suggested that the upstream convection of disturbances indicates that an absolute instability may be responsible for bubble flapping on this geometry.

Time-resolved surface pressure sensors have been recently employed in experiments on airfoils operating at low chord Reynolds numbers. Yarusevych et al. (2008) demonstrated that time-resolved surface pressure sensors can be used to measure disturbance amplification in the separated shear layer over a low Reynolds number airfoil and to identify the central frequency of disturbance amplification. Gerakopulos and Yarusevych (2012) developed an embedded surface pressure sensor array for low Reynolds number airfoil experiments and verified the accuracy of this system against hot-wire measurements. Using this array, they showed that measurements from embedded pressure sensors below the separation bubble on a low Reynolds number airfoil agree qualitatively with those obtained in the separation bubbles formed on other geometries; specifically, the development of disturbance fluctuations contained a characteristic maximum just upstream of the reattachment location, a frequency band of amplified disturbances could be identified, and a surface pressure fluctuation convective speed of approximately 50% of the edge velocity was measured. It was further noted that when separation occurs without subsequent reattachment, surface pressure fluctuations have significantly lower amplitudes than when a separation bubble forms and that the RMS surface pressure distributions do not exhibit a characteristic maximum along the streamwise coordinate. With the capabilities of this pressure sensor array established, it can be used to perform a detailed parametric study of flow development over an airfoil at low Reynolds numbers.

The purpose of this investigation is to establish the dependence of separation and transition characteristics over an airfoil at low Reynolds numbers on the Reynolds number and angle of attack. Measurements of mean and fluctuating pressure from mean static pressure taps and an array of embedded surface pressure sensors are used to complete a parametric study of flow development over a NACA 0018 airfoil for $50{,}000 \leq Re \leq 250{,}000$ and $0° \leq \alpha \leq 21°$. The results provide a comprehensive data set for various quantities related to separated shear layer development, including separation bubble location, central instability frequency, disturbance amplification rates, and pressure fluctuation convection speeds.
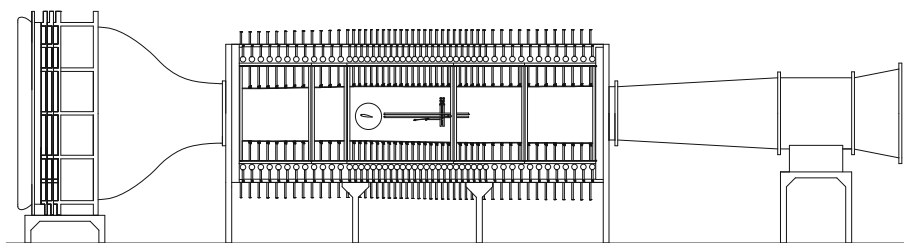
2 Experimental setup

Experiments were conducted in an adaptive-wall, open-return, suction-type wind tunnel at the University of Waterloo (Fig. 2). Four steel screens and a section of aluminum honeycomb upstream of a 9:1 contraction are used to condition the incoming flow. The test section has a width of 0.61 m and a height of 0.89 m. The test section walls were set in a straight and parallel configuration for this investigation. The free-stream speed was set to within 2.5% based on the pressure difference across the contraction section required to obtain the desired speed at the location of the model in an empty test section. The free-stream turbulence intensity over the Reynolds number range of interest was measured using a single normal wire hot-wire probe, and the results are presented in Table 1.

Flow over a NACA 0018 airfoil is considered in this investigation. This profile was selected because there is a comparatively limited amount of data available for the thick airfoil profiles required to withstand large forces in certain designs, such as low Reynolds number wind turbine blades (Yarusevych et al. 2009; Timmer 2008; Nakano et al. 2007). Furthermore, flow regimes representative of those observed on other airfoil sections in low Reynolds number flows can be observed over this geometry. The airfoil model, illustrated in Fig. 3, is made of aluminum and has a chord length of 200 mm and a span of 600 mm. End plates and end caps, depicted in Fig. 3, were installed on the model to mitigate end effects. Circular end plates with a diameter of $2.25c$, extending $0.8c$ downstream of the trailing edge, and with a spanwise spacing of $2.0c$ were used. Based on spanwise surface pressure measurements, it was established that this design provides mean spanwise uniformity to within 2.5% (Boutilier and Yarusevych 2012). The angle of attack of the model was set using a digital protractor with an angular resolution of 0.1°. The aerodynamic zero angle of attack was chosen such that it produced close agreement in mean suction-side surface pressure distributions at equal positive and negative angles of attack.

Sixty-five static pressure taps of 0.4-mm diameter were installed along the airfoil chord in two rows, offset in the spanwise direction by 1 cm, as shown in Fig. 3. Mean static pressure taps were multiplexed to a pressure

Table 1 Measured free-stream turbulence intensity over the Reynolds number range of interest

Re	$\tilde{u}/U_\infty$ (%)
50,000	0.19
100,000	0.19
150,000	0.19
200,000	0.18
250,000	0.16
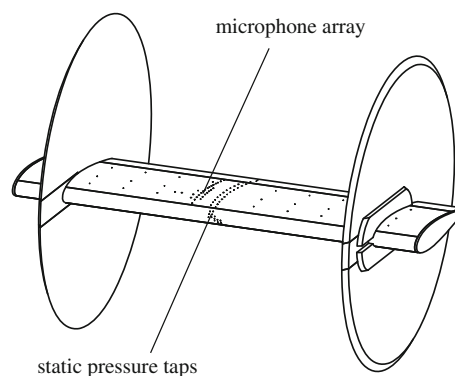
Fig. 3 Airfoil model

transducer using mechanical Scanivalve units. For $50,000 \leq Re \leq 150,000$, a Lucas Schaevitz P3061-2WD pressure transducer with a full scale range of 500 Pa was used, whereas for $150,000 < Re \leq 250,000$, a Scanivalve ZOC33 digital pressure scanner transducer with a full scale range of 2,500 Pa was used. The uncertainty in mean surface pressure measurements is estimated to be less than 3% of the free-stream dynamic pressure.

The fluctuating component of surface pressure was measured using an array of pressure sensors installed in the upper surface of the model along two streamwise rows, offset in span by 1 cm, and identified in Fig. 3. This array consisted of twenty-two Panasonic WM-62C omnidirectional back electret condenser microphones, flush mounted on the inner surface of the 1-mm-thick airfoil skin, concentric with 0.8-mm diameter ports. The array extends over the range $0.08 \leq x/c \leq 0.73$. Each microphone output voltage was passed through an amplifier circuit built into the airfoil model, with an amplifier gain of approximately

13 dB. Simultaneous sampling of up to eight channels was accomplished using a National Instruments PCI-4472 data acquisition card. Output voltages were sampled at 40 kHz and low-pass-filtered at 20 kHz. Each microphone and amplifier channel was calibrated in an anechoic chamber against a Brüel and Kjær 4192 working-standard reference microphone. Calibration was performed with the microphones installed concentric with 0.8-mm diameter holes in a 1-mm-thick plate, to simulate the configuration once installed in the model. The results showed a uniform frequency response up to approximately 4 kHz (Gerakopulos and Yarusevych 2012). Further details on the surface pressure sensor array installation, amplifier circuit, calibration procedure, and data processing techniques are provided in Gerakopulos and Yarusevych (2011). The uncertainty in RMS pressure measurements is estimated to be less than 3% of the free-stream dynamic pressure.

3 Results

Detailed measurements were performed for $100{,}000 \leq Re \leq 250{,}000$ and $0° \leq \alpha \leq 21°$. In addition, to investigate the effect of Reynolds number on specific flow characteristics over a broader range, measurements were completed for $Re = 50{,}000$ and $75{,}000$ at selected angles of attack.

Mean surface pressure distributions can be used to estimate separation bubble characteristics over low Reynolds number airfoils and to compute the pressure force component of lift (Tani 1964; O'Meara and Mueller 1987; Schmidt and Mueller 1989). Representative upper surface pressure distributions measured for $Re = 150{,}000$ are presented in Fig. 4 for selected angles at which a separation bubble forms. A pressure plateau can be identified in each of these distributions, which has been shown to occur in the vicinity of the separated flow region (Tani 1964). This behavior makes estimating the separation bubble size and location from mean surface pressure measurements possible. These locations were estimated by a similar procedure to that described in Gerakopulos et al. (2010) and illustrated in Fig. 5. The separation and transition points were estimated as the start and end of the region of nearly constant surface pressure downstream of the suction peak (O'Meara and Mueller 1987). The reattachment point was similarly estimated as the end of the region of enhanced rate of pressure recovery downstream of the transition point (O'Meara and Mueller 1987). As sketched in Fig. 5, these points were estimated from linear fits to the surface pressure data just upstream of the separation point, in the pressure plateau, in the rapid pressure recovery region, and just downstream of the reattachment point. The estimated uncertainty in stated locations of separation, transition, and
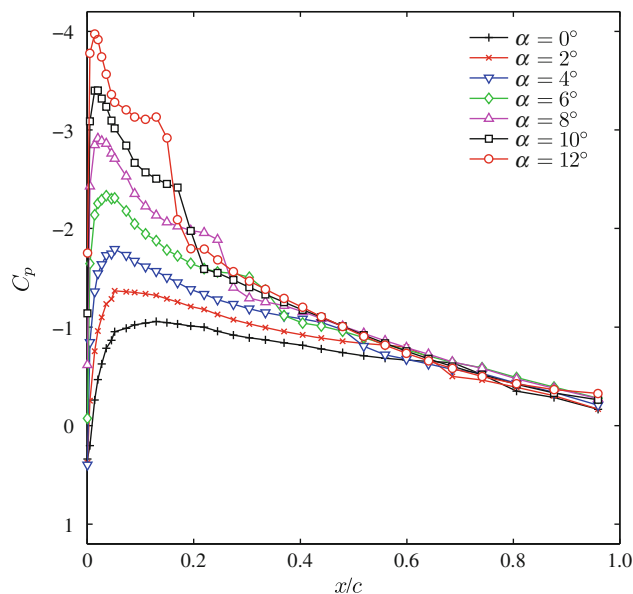

Fig. 4 Upper surface mean pressure distributions for a selection of angles of attack at which a separation bubble forms at $Re = 150{,}000$
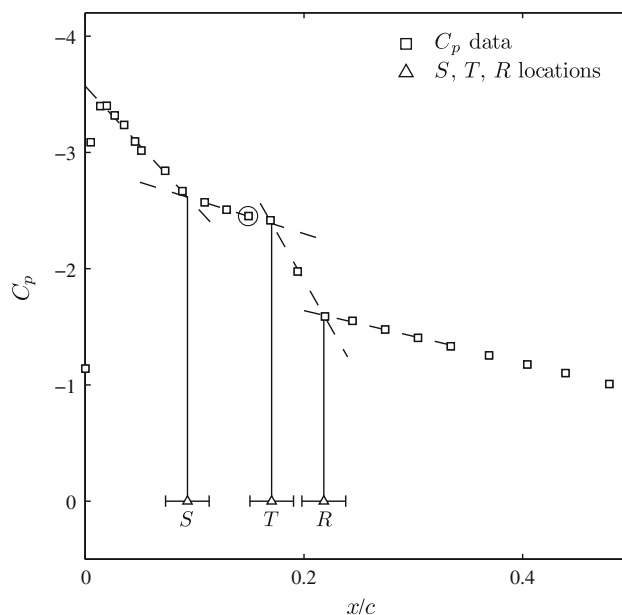
Fig. 5 Method employed for estimating separation, transition, and reattachment locations from mean surface pressure data. Data for $Re = 150{,}000$ and $\alpha = 10°$ are used in this example. Locations of separation, transition, and reattachment are indicated by S, T, and R, respectively, with 2% uncertainty bands shown. The location, just upstream of the transition point, at which the edge velocity is estimated is indicated by a *circle*

reattachment is 2% of the chord, that is, to within a band three static pressure taps wide. The method for estimating locations of separation, transition, and reattachment was verified by comparison with hot-wire measurements for $Re = 100{,}000$ and $\alpha = 0°$, $5°$, and $10°$. Furthermore, Gerakopulos et al. (2010) shows that measurements of
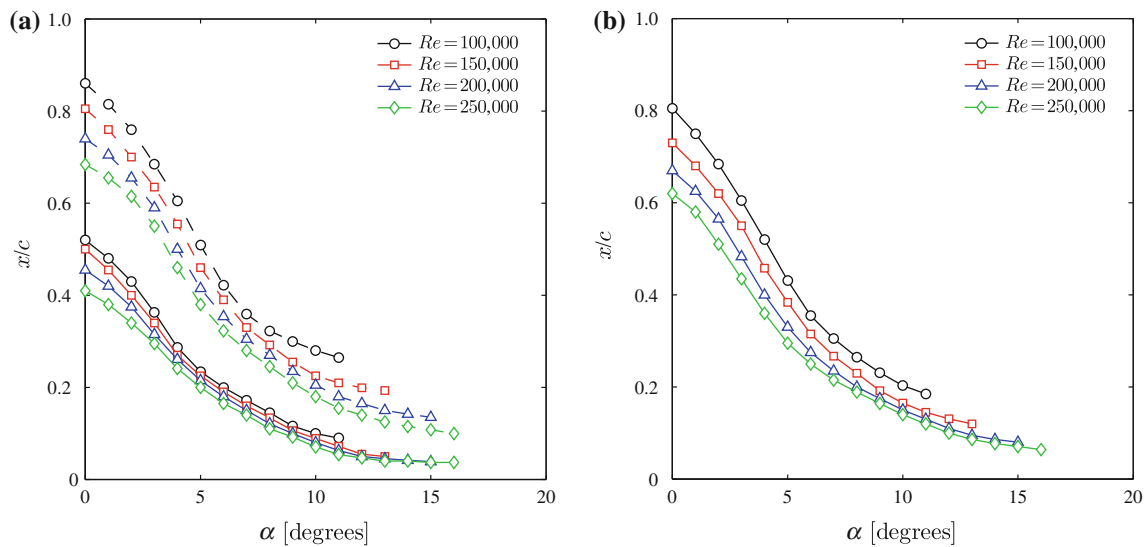
Fig. 6 Estimated mean locations of **a** separation (*solid curves*) and reattachment (*dashed curves*) as well as **b** transition

separation and reattachment locations on this model at a chord Reynolds number of 160,000 accurately agree with those reported by Nakano et al. (2007). Estimates of separation, transition, and reattachment locations obtained in the present investigation are plotted in Fig. 6.

Figure 6 shows qualitatively common trends for the size and position of a separation bubble on an airfoil at low Reynolds numbers (O'Meara and Mueller 1987). Specifically, on the average, the separation bubble moves upstream and decreases in length as the angle of attack or Reynolds number is increased. As seen in Fig. 6, the upstream movement of the separation point with increasing Reynolds number is more gradual than the upstream movement of the transition and reattachment points. Furthermore, it can be seen that the separation bubble location has a stronger dependence on the angle of attack than on the Reynolds number. For each Reynolds number, the variation in separation, transition, and reattachment locations with angle of attack is similar.

The dependence of separation bubble length on angle of attack and Reynolds number is shown in Fig. 7. The results suggest that the length of the separation bubble changes more significantly with angle of attack than with Reynolds number. Figure 6a shows that the decreasing separation bubble length with increasing angle of attack and Reynolds number results from a higher rate of upstream movement of the reattachment point with Reynolds number and angle of attack than of the separation point.

Measurements of mean surface pressure distributions can also be used to estimate the edge velocity in the separated shear layer. The edge velocity was estimated from the mean surface pressure coefficient measured just upstream of the transition point as $U_e/U_\infty \approx \sqrt{1 - C_p}$,

and the results are presented in Fig. 8a. For each Reynolds number, the edge velocity increases with angle of attack up to the stall angle. At this angle, the edge velocity decreases substantially and varies more gradually with further increases in the angle of attack. The stall angle was found to increase from 12° at $Re = 100,000$ to 16° at $Re = 250,000$. Comparing flow conditions at which reattachment occurs or at which the airfoil is stalled, it can be seen from Fig. 8a that the ratio of edge velocity to free-stream speed is nearly constant with Reynolds number.

Lift coefficients, computed from mean surface pressure distributions, are presented in Fig. 8b. No blockage corrections have been applied to these data; however, it was shown through a wall streamlining study on this model at moderate blockage ratios (4–8%) that simple blockage correction methods (see, e.g., Barlow et al. 1999) can accurately adjust lift coefficients for conditions at which a separation bubble forms (Boutilier and Yarusevych 2012). For angles of attack less than approximately 6°, a high lift slope is observed at each Reynolds number. For these angles, the separation bubble forms sufficiently far downstream that the increased lift compared to fully turbulent flow over the airfoil, produced by the pressure plateau at the location of the separation bubble, is greater than the reduction in lift produced by the diminished suction peak resulting from separation (Fig. 4). At these low angles, the lift slope rises with angle of attack. This is consistent with Figs. 7a and 8a, which show that between an angle of attack of 2° and 5°, the rate of upstream movement of the separation bubble increases, resulting in a higher rate of rise of the suction pressure in the separation bubble, and thus, a higher lift slope. However, for $\alpha \gtrsim 6°$, the separation bubble forms near the leading edge and causes a
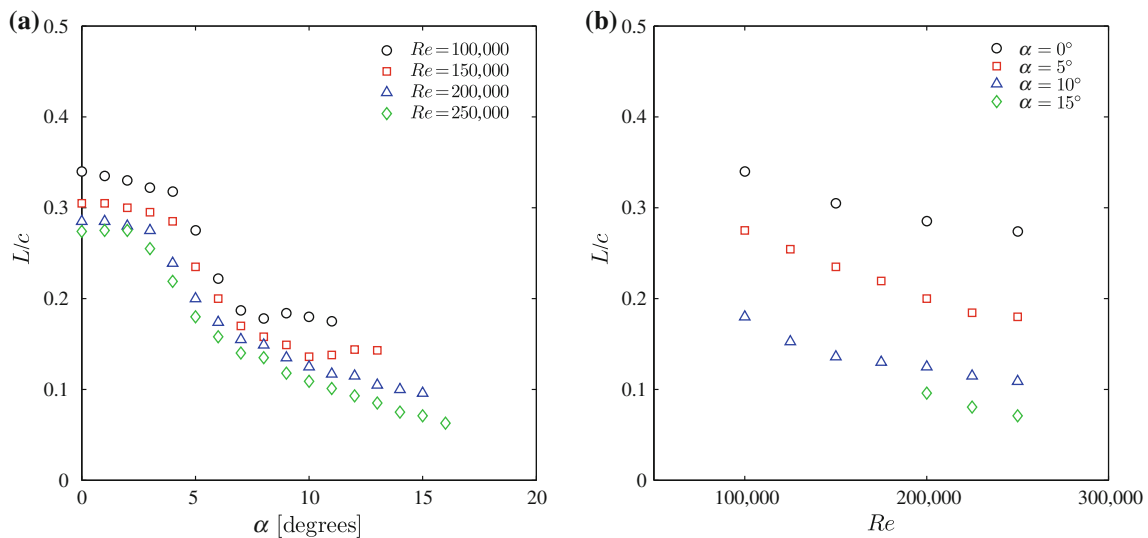
Fig. 7 Variation in separation bubble length with **a** angle of attack and **b** Reynolds number
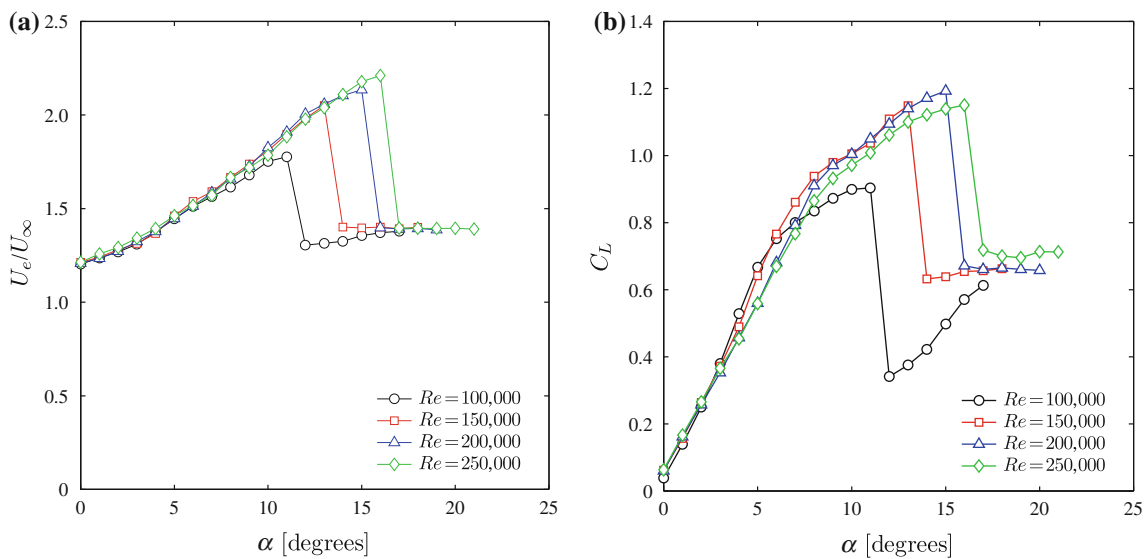

Fig. 8 Variation of **a** edge velocity just upstream of the transition point and **b** lift coefficient, with angle of attack

significant reduction in the maximum suction pressure on the upper surface. This results in lift slopes of less than half those observed at lower angles. Above the stall angle, the turbulent shear layer no longer reattaches, resulting in a significant reduction in lift.

Mean surface pressure measurements provide estimates of the location of the separated flow, edge velocity in the separated shear layer, and lift. However, if characteristics of the transition process in the separated shear layer are of interest, the time-varying component of surface pressure can provide further insight. Transition in a separated shear layer exposed to low magnitude free-stream disturbances proceeds by the amplification of background velocity and pressure fluctuations over a band of unstable frequencies

(Dovgal et al. 1994; Boiko et al. 2002). The ability to estimate or measure this frequency band is important in low Reynolds number active flow control systems that target these frequencies acoustically or mechanically to accelerate the transition process (Gad-el-Hak 1990; Rist et al. 2002; Nishioka et al. 1990; Yarusevych et al. 2005; Jones et al. 2008). Figure 9 presents energy spectra of pressure fluctuations computed from time-resolved surface pressure measurements at a microphone location between the separation and transition points for $Re = 150,000$. This plot illustrates the band of frequencies being amplified in the shear layer. For a given angle of attack and Reynolds number, this band of frequencies can be observed at various spatial locations and is most prominent with respect to
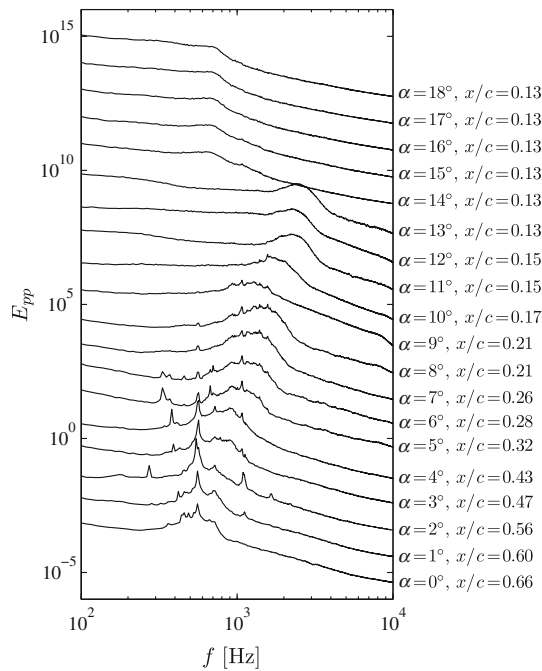
Fig. 9 Energy spectra of surface pressure fluctuations at $Re = 150,000$, normalized by the total energy content. For clarity, spectra at successive angles of attack are offset by increasing orders of magnitude

the background disturbances just upstream of the transition point. The dominant frequency of disturbance amplification in the shear layer was estimated from the microphone data for a range of Reynolds numbers and angles of attack. The results are compiled in Fig. 10. The uncertainty in these values, resulting from the width of the spectral peak and local maxima within the band of unstable frequencies, is estimated to be less than 5%.
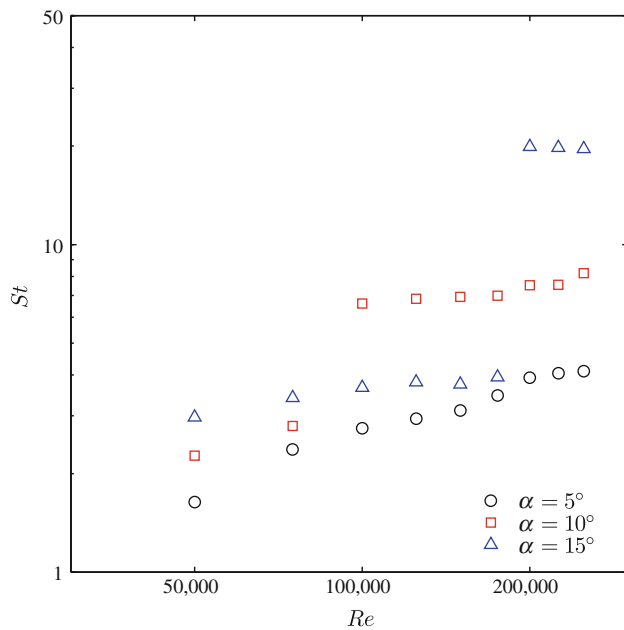
As seen in Fig. 10a, for conditions at which a separation bubble forms, the central frequency of disturbance amplification increases with Reynolds number and angle of attack. Comparing Figs. 8 and 10, it can be seen that bubble bursting results in a significant, abrupt decrease in the shear layer frequency. The shear layer frequency also varies more gradually under stalled conditions than when reattachment occurs. The variation of instability frequency with Reynolds number at particular angles of attack is presented in Fig. 10b. Yarusevych et al. (2009) showed, based on data for several airfoils at low Reynolds numbers, that at a fixed angle of attack, the shear layer frequency varies approximately as $f_0 \propto Re^n$. This is in agreement with the observed trend in the wake shear layer frequency measured over circular cylinders for Reynolds numbers based on diameter between 1,000 and 50,000 (Bloor 1964; Prasad and Williamson 1997; Thompson and Hourigan 2005). For low Reynolds number airfoils, Yarusevych et al. (2009) estimated exponent values in the range $0.9 \lesssim n \lesssim 1.9$ based on data for LA2573A (LeBlanc et al. 1989), NACA 0012 (Huang and Lin 1995), NACA 0025 (Yarusevych et al. 2009), and SD 7003 (Burgmann and Schröder 2008) airfoils. The power-law fits plotted in Fig. 10b for the NACA 0018 airfoil predict values of n in the range observed by Yarusevych et al. (2009). However, it can be seen that airfoil geometry and angle of attack have a strong effect on the value of n.

The central frequency of disturbance amplification is non-dimensionalized by the projected model height and free-stream velocity in Fig. 11, forming a Strouhal number for shear layer instability. Consistent with observations for a NACA 0025 airfoil by Yarusevych et al. (2009), the Strouhal number varies more gradually with angle of attack
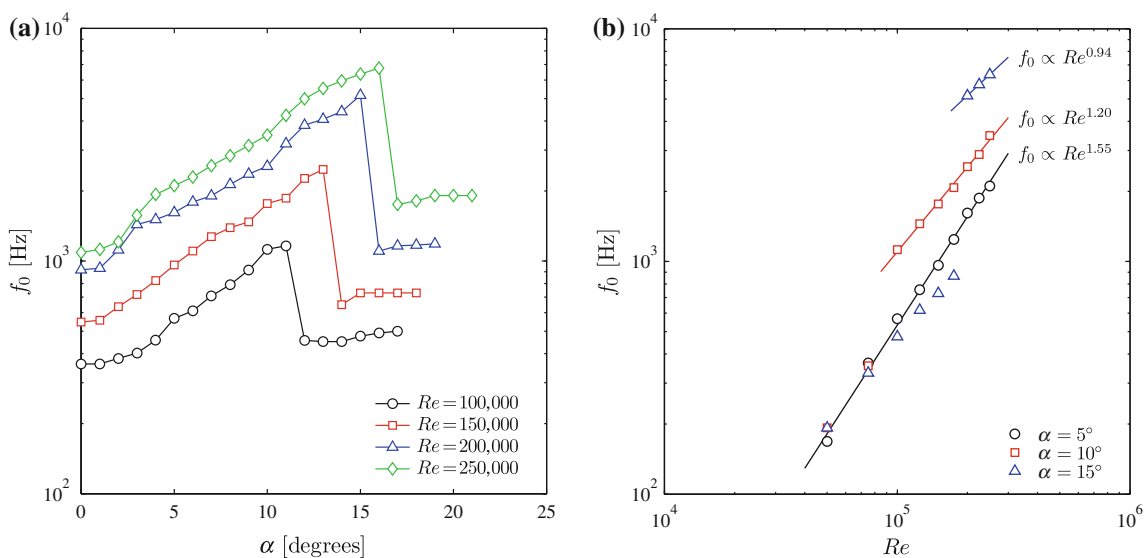
Fig. 10 Variation of the central frequency of disturbance amplification with **a** angle of attack and **b** Reynolds number
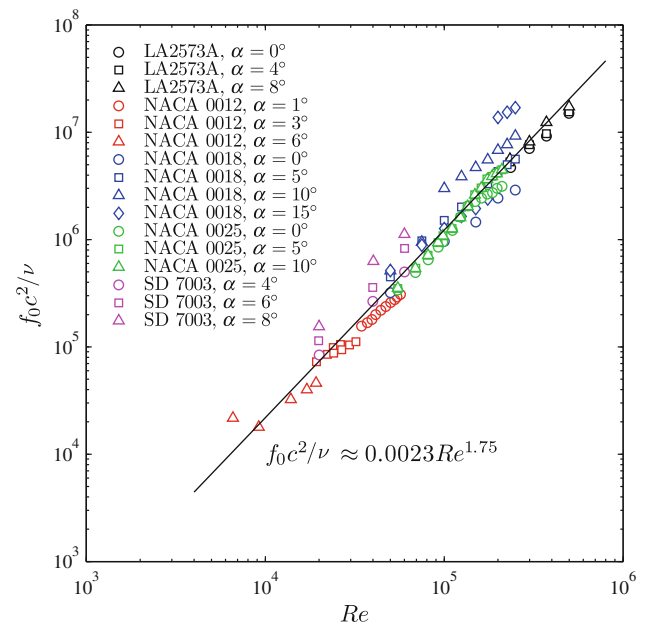
Fig. 11 Strouhal number for the central frequency of disturbance amplification


Fig. 12 Non-dimensional central frequency of disturbance amplification for various airfoil geometries operating at low Reynolds numbers. Data are from the following sources: LA2573A, LeBlanc et al. (1989); NACA 0012, Huang and Lin (1995); NACA 0018, present investigation; NACA 0025, Yarusevych et al. (2009); SD 7003, Burgmann and Schröder (2008)

at higher Reynolds numbers, for which a separation bubble forms. Furthermore, values of the Strouhal number vary more significantly between angles of attack for conditions at which a separation bubble forms and are more similar in magnitude for stalled conditions.

An alternative non-dimensional form of the instability frequency is the Roshko number based on the model chord length, that is, $f_0 c^2 / \nu$, which is the product of the Strouhal number and the Reynolds number (Huang and Lin 1995). In this form, the shear layer frequency is scaled by the fluid properties, allowing comparison of measurements over airfoils of different sizes in both water and air. The variation of Roshko number with chord Reynolds number for several airfoils operating at low Reynolds numbers is presented in Fig. 12. By this scaling, all of the data reside within a band of non-dimensional frequencies, which increases with Reynolds number as $f_0 c^2 / \nu \propto Re^{1.75}$. This indicates that the shear layer instability frequency is primarily determined by the Reynolds number rather than the specific airfoil geometry or angle of attack. The power-law fit in Fig. 12 provides a method for estimating the order of magnitude of the shear layer instability frequency, which is of practical importance, for example, in selecting sensors for flow measurement systems or flow control feedback devices. However, the power-law fit in Fig. 12 only identifies an approximate trend in the magnitude of the shear layer instability frequency with Reynolds number, not the expected behavior for a particular geometry and angle of attack. This is evident from the deviation in the data in Fig. 12 within a band an order of magnitude wide and from

the significantly more accurate power-law fits in Fig. 10b. The NACA 0018 and SD 7003 airfoil data show increasing deviation from the trend line with angle of attack for cases at which a separation bubble forms (i.e., all data point for the SD 7003 and those conditions plotted in Fig. 7 for the NACA 0018). The most significant variation is observed for the NACA 0018 airfoil at $Re \geq 200{,}000$ and $\alpha = 15°$, the highest angle of attack out of all of the data sets presented. Figure 12 suggests that, although the effects of the airfoil geometry and angle of attack on the Roshko number are secondary to those of the Reynolds numbers, they are still significant.

The NACA 0018 and NACA 0025 data sets in Fig. 12 include measurements at stalled conditions. For the NACA 0025 data, these conditions were observed for $Re \lesssim 100{,}000$ (Yarusevych et al. 2009). For both of these airfoil profiles, the shear layer instability frequency closely follows the power-law trend line in Fig. 12 for each angle of attack. The value of $n = 1.75$ in the $f_0 c^2 / \nu \propto Re^n$ scaling for all the data sets presented in Fig. 12 is similar to the values between 1.83 and 1.91 determined by Yarusevych et al. (2009) for the NACA 0025 airfoil under stalled conditions. This suggests that the scaling exponent, n, is only weakly dependent on the angle of attack and specific airfoil profile for stalled conditions. It is interesting that, despite the variation in the frequency scaling exponent between 0.9 and 1.9 for conditions at which a separation bubble forms, the significant variation in the Reynolds number below

**Fig. 13** Spatial variation of RMS surface pressure at $Re = 150,000$
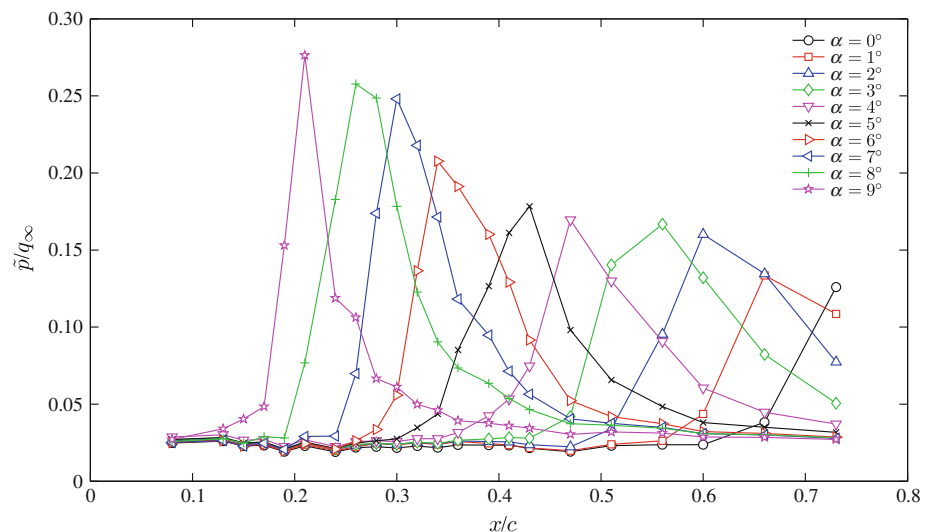
which stall occurs at a particular angle of attack allows for an approximate scaling with $Re^{1.75}$ for conditions with and without reattachment.

The variation of RMS surface pressure on the upper surface of the airfoil is presented in Fig. 13 for the representative case of $Re = 150,000$. For each angle of attack, the RMS surface pressure is at a background level near the leading edge of the model. Downstream, RMS surface pressure increases at a high rate for a short distance, reflecting the growth of disturbances in the separated shear layer (Mabey 1972; Dovgal et al. 1994). This amplification occurs between the separation and transition locations, as seen by comparison with Fig. 6. Agreeing with prior studies employing surface pressure sensors to examine separation bubble development (Gerakopulos and Yarusevych 2012; Mabey 1972; Hudy et al. 2003; Farabee and Casarella 1986; Driver et al. 1987; Lee and Sung 2001; Cherry et al. 1984; Weibust et al. 1987), including work on this model, the location of maximum RMS surface pressure corresponds to a location between the mean transition and reattachment points. The amplitude of surface pressure fluctuations decays downstream of this peak. The relatively high rate of decline of the RMS surface pressure just downstream of the peak is attributed to the loss of coherence of pressure fluctuations as energy content is distributed over a broader band of frequencies in the final breakdown to turbulence. The lower rate of decline farther downstream may result from continued thickening of the shear layer. The upstream movement of the transitional separated shear layer with angle of attack, identified in relation to Fig. 6, is evident in Fig. 13. From this plot, it can also be seen that, as the angle of attack increases, the maximum amplitude of RMS surface pressure fluctuations and the maximum spatial growth rate of RMS surface pressure fluctuations also increase. This variation is explored further below.

It should be noted that, although the stall angle at $Re = 150,000$ is $\alpha = 13°$, in Fig. 13, RMS surface pressure plots have only been presented for $0° \leq \alpha \leq 9°$. As the separation bubble continues to move upstream and decrease in length with increasing angle of attack, a portion of the transitional separated shear layer moves upstream of the sensor array and the bubble occupies a region with very few sensors. As a result, for certain flow conditions, neither the maximum RMS surface pressure nor the rate of disturbance amplification can be estimated reliably. Flow conditions for which values of maximum surface pressure and growth rate cannot be estimated reliably have been excluded. It has also been shown that at post-stall angles of attack, the increased distance between the shear layer core and the airfoil surface results in relatively low-amplitude pressure fluctuations (Gerakopulos and Yarusevych 2012; Boutilier 2011). These data can be used to determine whether shear layer reattachment occurs and to estimate the central frequency of disturbance amplification, but do not provide reasonable estimates of disturbance amplification rate or convection speed. For this reason, spatial distributions of RMS surface pressure have not been included for post-stall angles of attack; however, these data have been used to estimate central frequencies of disturbance amplification and maximum RMS surface pressures.

Figure 14a presents the variation of the maximum measured RMS surface pressure over the angle of attack and Reynolds number range investigated. Figure 13a illustrates that, for conditions at which a separation bubble forms (data for $\alpha \leq 9°$ in this plot), the spatial resolution of the microphone array causes relatively high uncertainty in the estimate of the maximum RMS surface pressure. It is estimated that, for conditions at which a separation bubble forms, the maximum measured RMS surface pressure
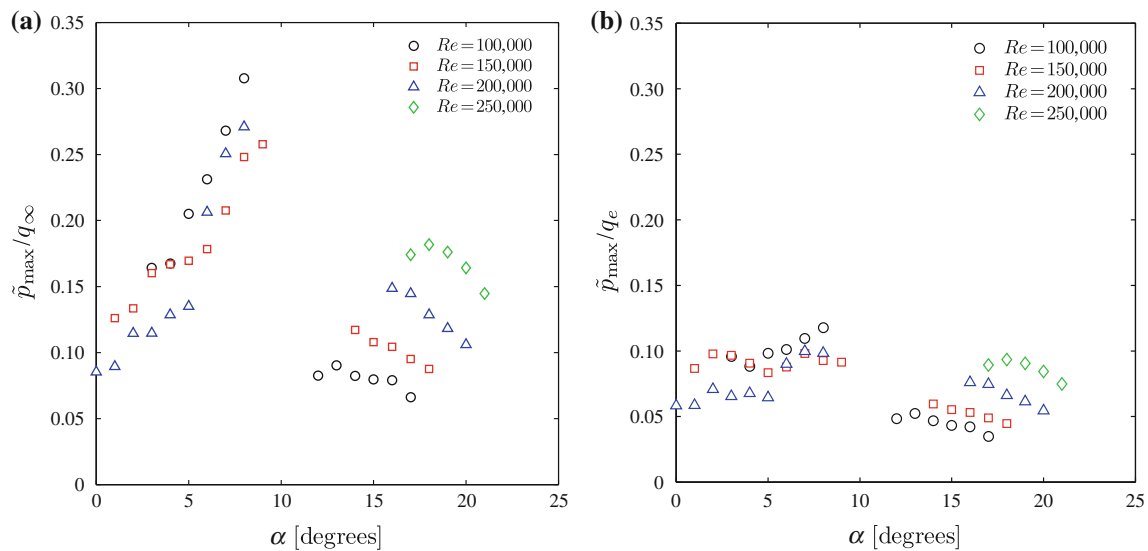
Fig. 14 Maximum RMS surface pressure normalized by **a** free-stream dynamic pressure and **b** dynamic pressure based on edge velocity

could be up to $0.08q_\infty$ lower than the actual maximum RMS surface pressure. At post-stall angles of attack, the RMS surface pressure varies gradually in the streamwise direction. As a result, the estimated uncertainty in the stated maximum RMS surface pressure for these angles is less than $0.03q_\infty$. Due to the high uncertainty in maximum RMS surface pressure for separation bubble conditions, the variation in maximum RMS surface pressure with Reynolds number at a fixed angle of attack cannot be compared. However, the variation in maximum RMS surface pressure with angle of attack has significance. The value of $\tilde{p}_{max}/q_\infty$ increases from less than 0.10 to greater than 0.25 between $\alpha = 0°$ and $\alpha = 8°$, demonstrating that the amplitude of surface pressure fluctuations attained before the final breakdown to turbulent flow is dependent on the angle of attack. The length of the laminar separated shear layer must, therefore, be affected by both the disturbance amplification rate and the threshold amplitude of pressure fluctuations at which transition occurs. The values of $\tilde{p}_{max}/q_\infty$ presented in Fig. 14a are between approximately 0.05 and 0.30. These are significantly higher than the values between 0.04 and 0.1 observed by Mabey (1972) for separation bubbles forming on splitter plates with fences, forward facing steps, and backward facing steps. However, the data presented by Mabey (1972) show that the maximum RMS surface pressure in a separation bubble does depend on the geometry over which the bubble forms. For lower angles of attack, the airfoil geometry and edge velocity in the vicinity of the separation bubble are most similar to those of the zero-incidence geometries considered by Mabey (1972), resulting in values of maximum RMS surface pressure that are closest to the range reported by Mabey (1972).

The edge velocity in the separation bubble forming over an airfoil can be significantly higher than in those forming over splitter plates with fences, forward facing steps, and backward facing steps. It may, therefore, be more appropriate to non-dimensionalize the maximum RMS surface pressure by a dynamic pressure based on the edge velocity in the separated shear layer. Data have been non-dimensionalized in this way in Fig. 14b. The range of maximum RMS surface pressures for conditions at which a separation bubble forms is reduced to $0.05 \lesssim \tilde{p}_{max}/q_\infty \lesssim 0.12$, similar to the range based on q_∞ observed in the data of Mabey (1972) for separation bubbles on other geometries. This indicates that the amplitude that surface pressure fluctuations must attain in order to initiate the final breakdown to turbulence is strongly dependent on the dynamic pressure at the edge of the separated shear layer, rather than a fixed amplification ratio relative to the background disturbances.

The variation of maximum surface pressure with Reynolds number can be assessed at post-stall angles of attack (Fig. 14, data for $\alpha \geq 10°$). For these flow conditions, the maximum RMS surface pressure varies by less than 10% of the dynamic pressure over the sensor array. On the average, the magnitudes of the RMS surface pressure at post-stall angles decrease gradually with increasing angle of attack and increase with increasing Reynolds number. For stalled conditions, the surface pressure is strongly influenced by both the separated shear layer and the near wake development, with the latter contributing through recirculation of fluid from the wake into the separated flow region and through the higher surface pressure fluctuation magnitudes imposed on the model by coherent structures forming in the near wake. Hence, it is expected that the magnitude of surface pressure fluctuations will be related to velocity
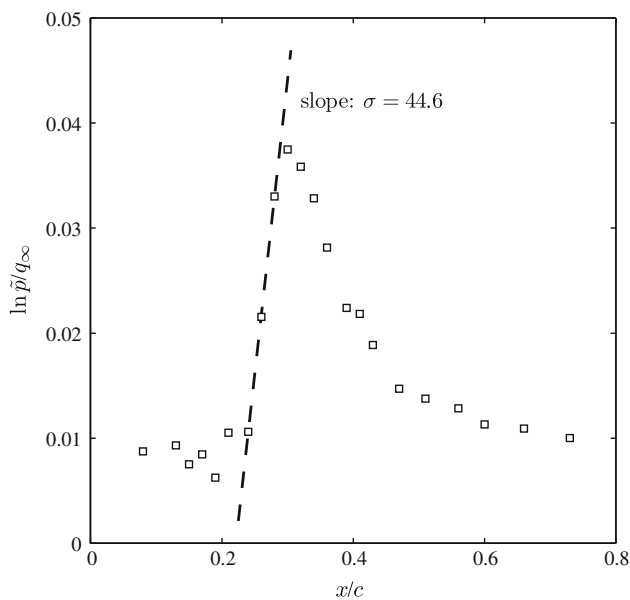
**Fig. 15** Sketch of σ calculation, shown for $Re = 150{,}000$ and $\alpha = 7°$

fluctuations in the separated shear layer and wake. Wake measurements for this model, presented by Yarusevych and Boutilier (2011), suggest that, as the Reynolds number increases, the magnitude of velocity fluctuations in the near wake also increases. This is believed to be responsible for the observed increase in the RMS surface pressure with increasing Reynolds number at post-stall angles in Fig. 14.

The spatial amplification rate of disturbances can also be estimated from RMS surface pressure distributions (Gerakopulos and Yarusevych 2012; Boutilier 2011). The value of σ is the estimated maximum slope of $\ln \tilde{p}/q_\infty$ versus x/c, representing an approximate rate of exponential disturbance growth. This definition is illustrated in Fig. 15 and is based on the exponential growth of modal components of pressure and velocity fluctuations assumed by linear stability theory. Although linear theory does not assume such growth for RMS quantities, defining σ in this way allows for a comparison with linear theory, as is common in studies on transitional separation bubbles (Lang et al. 2004; Rist et al. 1996, 2002; Jones et al. 2010). The variation of the spatial growth rate with Reynolds number and angle of attack is presented in Fig. 16, for conditions at which a separation bubble forms. The estimated uncertainty in these values is 20%, based on the combined uncertainty in RMS surface pressure measurements and the sensitivity of the reported σ value to the choice of data points included in the linear fit. Figure 16 shows that the spatial growth rate increases with both the Reynolds number and the angle of attack, providing a physical explanation for the accompanying decrease in the separation bubble length. It should be noted that, because the amplification rate of disturbances varies with

frequency, the growth rate of disturbances at the central frequency in the energy spectrum peak (Fig. 9) will be higher than the growth rate of the overall RMS pressure signal. The relative difference between these values was estimated by band-pass-filtering the pressure signals in a 5% wide band about the central frequency of the spectral peak and computing the growth rate based on RMS values of these data for $Re = 100{,}000$ and $\alpha = 0°$, $5°$, and $10°$. It was found that the modal RMS surface pressure growth rate at the frequency of maximum disturbance amplification was lower than the spatial amplification rate of RMS surface pressure by a factor of on the order of two (Boutilier 2011). However, the general trends in Fig. 16 were also observed for the modal component at the central frequency of disturbance amplification (Boutilier 2011).

Simultaneous time-resolved measurements of surface pressures can be used to estimate the average convection speed of pressure fluctuations in the shear layer (Gerakopulos and Yarusevych 2012; Hudy et al. 2003; Farabee and Casarella 1986; Cherry et al. 1984). In the present investigation, the convection speed has been estimated by a linear fit to the accumulated time lag between pressure signals at different spatial locations in the separation bubble. The time lag was determined as the time-delay corresponding to the maximum in the cross-correlation of microphone signals. The procedure for measuring convection speed is discussed in more detail by Gerakopulos and Yarusevych (2012). The convection speed physically represents the average speed of a growing disturbance wave packet propagating through the shear layer. Values of convection speed normalized by the free-stream speed are presented in Fig. 17a. The uncertainty in reported convection speeds is estimated to be 3.5% of the free-stream velocity. At low angles of attack, the measured convection speeds agree with the values of between approximately 50 and 60% of the free-stream velocity reported for the separation bubbles on blunt face splitter plates (Cherry et al. 1984) and backward facing steps (Farabee and Casarella 1986). However, as the angle of attack increases, convection speeds exceed this range. As with the $\tilde{p}_{max}/q_\infty$ data in Fig. 14a, the measured values from the present investigation match those measured on separation bubbles on geometries at zero incidence best at low angles of attack. It is expected that the differences at higher angles of attack are due to the higher edge velocities in the separated shear layer. The magnitudes of U_c/U_∞ reported here for relatively high angles of attack are similar to the value of 0.85 reported by Burgmann and Schröder (2008) for an SD 7003 airfoil at $\alpha = 8°$ for $Re = 40{,}000$ and $60{,}000$.

Convection speeds are normalized by the edge velocity in Fig. 17b. The convection speeds are reduced to the range $0.35 \lesssim U_c/U_e \lesssim 0.5$ by this non-dimensionalization. Yarusevych et al. (2009) found a narrower range of
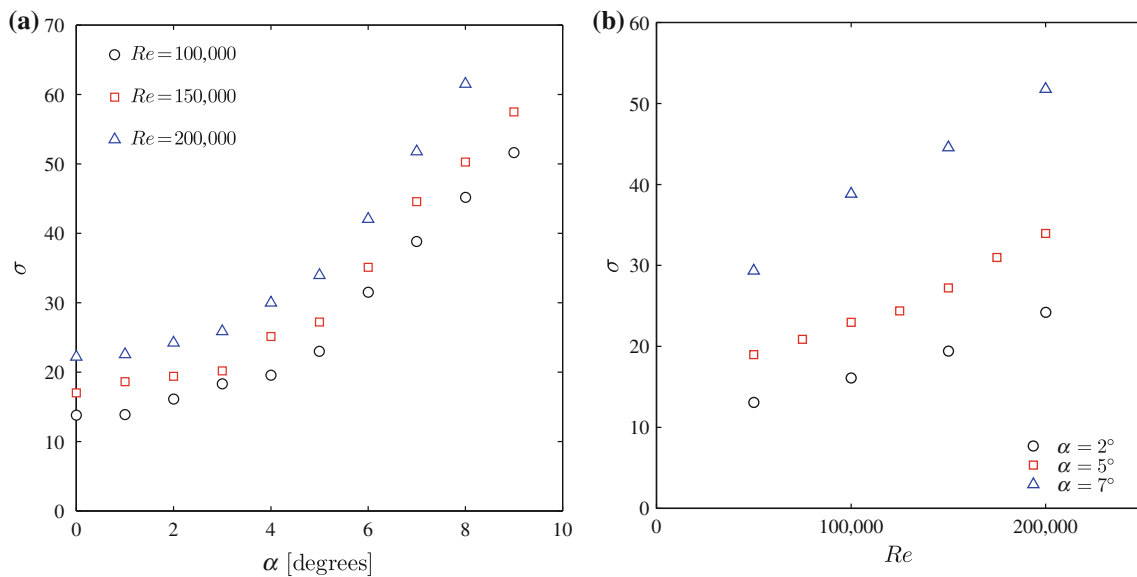
Fig. 16 Variation of spatial amplification rate of RMS surface pressure with **a** angle of attack and **b** Reynolds number
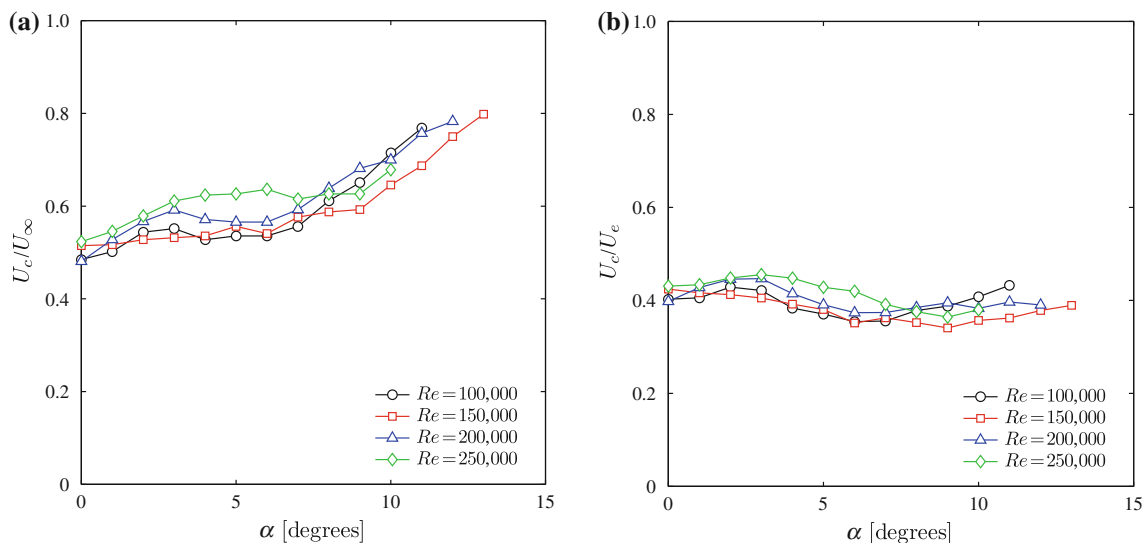
Fig. 17 Convection speed of pressure fluctuations, normalized by **a** free-stream speed and **b** edge velocity

values, between approximately 0.45 and 0.5, from a smaller data set primarily comprised of measurements at stalled conditions. They reasoned that this range of speeds corresponds to the average of the edge velocity and the maximum reverse flow speed, because that is the approximate speed of the fluctuation vorticity core at the mean velocity profile inflection point. The wider range of values observed in Fig. 17b suggests that U_c/U_e is lower when a separation bubble forms than when the shear layer does not reattach. These observations are consistent with theoretical findings from linear stability theory, which predicts phase speeds of approximately 0.5 for the

inviscid instability of a free shear layer that approaches zero velocity in one direction (Michalke 1965), and lower values from viscous analysis of separated shear layer profiles, with the value depending on factors including the maximum reverse flow speed, the distance of the profile inflection point from the wall, and the Reynolds numbers based on shear layer thickness (Dovgal et al. 1994). It is, therefore, reasonable to expect that, under stalled conditions, the convection speed will be closer to the phase speed value of $0.5U_e$, predicted for a free shear layer, and lower when a separation bubble forms. The range of U_c/U_e values observed here is also consistent with the
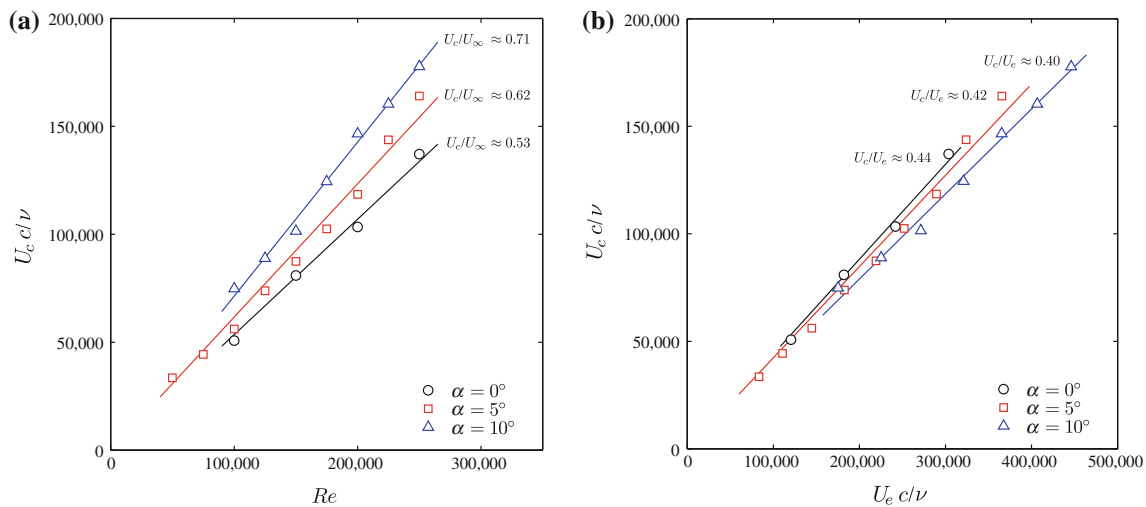
Fig. 18 Variation of convection speed of pressure fluctuations with **a** free-stream speed and **b** edge velocity

range of phase speeds predicted from linear stability analysis on analytical separated shear layer profiles by Dovgal et al. (1994).

The variation of convection speed with angle of attack and Reynolds number is further illustrated in Fig. 18. Figure 18 presents convection speed versus free-stream speed and edge velocity, with all speeds normalized by the constant c/ν. These parameters are effectively Reynolds numbers based on free-stream speed, edge velocity, and convection speed. In Fig. 18, linear trend lines have been plotted to illustrate the average values of convection speed over a range of angles of attack. However, Fig. 17 shows that at a given angle of attack, neither the convection speed normalized by the free-stream speed nor that normalized by the edge velocity is constant. Thus, the linear fits in Fig. 18 only indicate average trends. An average increase in U_c/U_∞ with Reynolds number is seen in Fig. 18a. The average variation of U_c/U_e with angle of attack (Fig. 18b) is significantly smaller than that of U_c/U_∞ (Fig. 18a), with the measured differences in U_c/U_e only slightly greater than the uncertainty in estimating this quantity. For the angles of attack presented in Fig. 18b, the linear fits show an average decline of U_c/U_e with angle of attack, away from the value of approximately 0.5 expected in free shear layers (Ho and Huerre 1984). This may be an indication that the deviation in flow instability in the separation bubble from that of a free shear layer increases as the angle of attack increases, due to an average reduction in the height of the shear layer core from the model surface as the angle of attack increases at low Reynolds numbers (Brendel and Mueller 1988). As a result, the difference between convection speeds in the separation bubble from that expected in a free shear layer increases.

4 Conclusion

Characteristics of separation and transition in the shear layer over a NACA 0018 airfoil at low Reynolds numbers were investigated using time-resolved surface pressure sensors. Measurements were performed for $50{,}000 \leq Re \leq 250{,}000$ and $0° \leq \alpha \leq 21°$. The results provide a comprehensive data set of characteristic separated shear layer parameters and reveal fundamental dependencies of these quantities on the Reynolds number and angle of attack.

Mean surface pressure distributions were used to estimate locations of separation, transition, and reattachment and to determine lift coefficients and edge velocities in the separated shear layer. As is common for airfoils under low Reynolds number conditions, the separation bubble moves upstream and decreases in length as the Reynolds number and angle of attack increase. The effect of this variation in the separation bubble size was evident in the lift curves, which showed a marked reduction in the lift slope for angles of attack at which the location of the separation bubble had a significant effect on the suction peak. The ratio of edge velocity to free-stream velocity was found to be approximately constant at a fixed angle of attack, when comparing velocities within a regime of separation with reattachment or separation without reattachment.

Simultaneous measurements of pressure signals at multiple x/c locations were used to estimate shear layer instability frequencies, spatial amplification rates, and convection speeds. Based on an analysis of the results obtained in the present investigation and previous studies on airfoils operating at low Reynolds numbers, a power-law correlation between the shear layer instability frequency and the Reynolds number of the form $f_0 c^2/\nu \propto Re^{1.75}$ was proposed. However, this correlation provides only an order

of magnitude estimate due to the influence of angle of attack and profile shape on the shear layer instability frequency. It was found that power-law fits for the instability frequency, specific to each airfoil profile and angle of attack, are more accurate, though less general. The ratio of the maximum RMS surface pressure to the free-stream dynamic pressure was found to increase significantly with angle of attack, to values approximately three times greater than those measured in separation bubbles over geometries other than airfoils (Mabey 1972). When normalized by the dynamic pressure based on the edge velocity, the range of non-dimensional maximum RMS surface pressures was reduced to between 0.05 and 0.12, consistent with the range observed for separation bubbles on other geometries. This suggests that the threshold amplitude of pressure fluctuations required to initiate the final turbulent breakdown is more strongly related to the edge velocity in the separated shear layer than to the free-stream velocity. Disturbance growth rates in the separation bubble increased with both angle of attack and Reynolds number, explaining the accompanying decrease in separation bubble length. Convection speeds of pressure fluctuations in the separation bubble were found to increase with angle of attack from approximately 50 to 90% of the free-stream speed. At lower angles of attack, the convection speeds are similar to those measured over backward facing steps, forward facing steps, and splitter plates with fences (Hudy et al. 2003; Farabee and Casarella 1986; Driver et al. 1987; Lee and Sung 2001) and, at higher angles of attack, are in agreement with the range of values measured over other low Reynolds number airfoils at similar angles of attack (Burgmann and Schröder 2008). This suggests that, similar to the findings for the maximum surface pressure fluctuations, the higher edge velocity in the separated region over an airfoil causes higher absolute values of the convection speed. When normalized by the edge velocity in the separated shear layer, the convection speeds are reduced to the range from approximately 35 to 50% of the edge velocity. This range of convection speeds, corresponding to disturbances in transitional separation bubbles, is wider than the range of 45–50% of the edge velocity reported by Yarusevych et al. (2009), based primarily on data for a stalled airfoil. The wider range observed in the present investigation is attributed to the shorter distance between the shear layer core and the airfoil surface when a separation bubble forms, causing greater differences in the flow instability behavior compared to that of a free shear layer. The ratios of convection speed to edge velocity measured in this investigation are in agreement with phase speeds predicted by Dovgal et al. (1994) from linear stability theory.

References

Bansmer S, Radespiel R, Unger R, Haupt M, Horst P (2010) Experimental and numerical fluid-structure analysis of rigid and flexible flapping airfoils. AIAA J 48(9):1959–1974

Barlow JB, Rae WH Jr, Pope A (1999) Low-speed wind tunnel testing, 3rd edn. Wiley, New York

Bloor MS (1964) The transition to turbulence in the wake of a circular cylinder. J Fluid Mech 19:290–303

Boiko AV, Grek GR, Dovgal AV, Kozlov VV (2002) The origin of turbulence in near-wall flows. Springer, Berlin

Boutilier MSH (2011) Experimental investigation of transition over a NACA 0018 Airfoil at a low Reynolds number, University of Waterloo, MASc thesis

Boutilier MSH, Yarusevych S (2012) Effects of end plates and blockage on low Re flows over airfoils. AIAA J (in press)

Brendel M, Mueller TJ (1988) Boundary-layer measurements on an airfoil at low Reynolds numbers. J Aircr 26(7):612–617

Burgmann S, Schröder W (2008) Investigation of the vortex induced unsteadiness of a separation bubble via time-resolved and scanning PIV measurements. Exp Fluids 45(4):675–691

Burgmann S, Brücker C, Schröder W (2006) Scanning PIV measurements of a laminar separation bubble. Exp Fluids 41(2):319–326

Carmichael BH (1981) Low Reynolds number airfoil survey vol. I, NASA CR 165803

Cherry NJ, Hillier R, Latour MEMP (1984) Unsteady measurements in a separated and reattaching flow. J Fluid Mech 144:13–46

Dovgal AV, Kozlov VV, Michalke A (1994) Laminar boundary layer separation: instability and associated phenomena. Prog Aerosp Sci 30(1):61–94

Driver DM, Seegmiller HL, Marvin JG (1987) Time-dependent behavior of a reattaching shear layer. AIAA J 25(7):914–919

Ellsworth RH, Mueller TJ (1991) Airfoil boundary layer measurements at low Re in an accelerating flow from a nonzero velocity. Exp Fluids 11(6):368–374

Farabee TM, Casarella MJ (1986) Measurements of fluctuating wall pressure for separated/reattached boundary layer flows. J Vib Acoust Stress Reliab Des 108(3):301–307

Gad-el-Hak M (1990) Control of low-speed airfoil aerodynamics. AIAA J 28(9):1537–1552

Gerakopulos R, Yarusevych S (2012) Novel time-resolved pressure measurements on an airfoil at a low Reynolds number. AIAA J (in press)

Gerakopulos R, Boutilier MSH, Yarusevych S (2010) Aerodynamic characterization of a NACA 0018 airfoil at low Reynolds numbers. In: Proceedings of the 40th AIAA fluid dynamics conference and exhibit, Chicago, Illinois, 28 June–1 July 2010, AIAA Paper No. 2010-4629

Hain R, Kähler CJ, Radespiel R (2009) Dynamics of laminar separation bubbles at low-Reynolds-number aerofoils. J Fluid Mech 630:129–153

Ho CM, Huerre P (1984) Perturbed free shear layers. Annu Rev Fluid Mech 16:365–422

Huang RF, Lin CL (1995) Surface flow and vortex shedding of an impulsively started wing. J Fluid Mech 441:265–292

Hudy LM, Naguib AM, Humphreys WM Jr (2003) Wall-pressure-array measurements beneath a separating/reattaching flow region. Phys Fluids 15(3):706–717

Jones LE, Sandberg RD, Sandham ND (2008) Direct numerical simulations of forced and unforced separation bubbles on an airfoil at incidence. J Fluid Mech 602:175–207

Jones LE, Sandberg RD, Sandham ND (2010) Stability and receptivity characteristics of a laminar separation bubble on an aerofoil. J Fluid Mech 648:257–296

Laitone EV (1997) Wind tunnel tests of wings at Reynolds numbers below 70,000. Exp Fluids 23:405–409

Lang M, Rist U, Wagner S (2004) Investigations on controlled transition development in a laminar separation bubble by means of LDA and PIV. Exp Fluids 36(1):43–52

LeBlanc P, Blackwelder R, Liebeck R (1989) A comparison between boundary layer measurements in a laminar separation bubble flow and linear stability theory calculations. In: Proceedings of the low Reynolds number aerodynamics conference, Notre-Dame, Indiana, 5–7 June 1989, pp 189–205

Lee I, Sung HJ (2001) Characteristics of wall pressure fluctuations in separated and reattaching flows over a backward-facing step: part I. Time-mean statistics and cross-spectral analysis. Exp Fluids 30(3):262–272

Lissaman PBS (1983) Low-Reynolds-number airfoils. Annu Rev Fluid Mech 15:223–239

Mabey DG (1972) Analysis and correlation of data on pressure fluctuations in separated flow. J Aircr 9(9):642–645

Marchman JF (1987) Aerodynamic testing at low Reynolds numbers. J Aircr 24(2):107–114

Michalke A (1965) On spatially growing disturbances in an inviscid shear layer. J Fluid Mech 23(3):521–544

Mueller TJ (1985) Low Reynolds number vehicles. AGARDograph 288

Mueller TJ, Batill SM (1982) Experimental studies of separation on a two-dimensional airfoil at low Reynolds numbers. AIAA J 20(4):457–463

Mueller TJ, DeLaurier JD (2003) Aerodynamics of small vehicles. Annu Rev Fluid Mech 35:89–111

Nakano T, Fujisawa N, Oguma Y, Takagi Y, Lee S (2007) Experimental study on flow and noise characteristics of NACA0018 Airfoil. J Wind Eng Ind Aerodyn 95:511–531

Nishioka M, Asai M, Yoshida S (1990) Control of flow separation by acoustic excitation. AIAA J 28(11):1909–1915

O'Meara MM, Mueller TJ (1987) Laminar separation bubble characteristics on an airfoil at low Reynolds numbers. AIAA J 25(8):1033–1041

Paterson RW, Vogt PG, Fink MR, Munch CL (1973) Vortex noise of isolated airfoils. J Aircr 10(5):296–302

Pelletier A, Mueller TJ (2000) Low Reynolds number aerodynamics of low-aspect-ratio thin/flat/cambered-plate wings. J Aircr 37(5):825–832

Prasad A, Williamson CHK (1997) The instability of the shear layer separating from a bluff body. J Fluid Mech 333:375–402

Rist U, Maucher U (2002) Investigations of time-growing instabilities in laminar separation bubbles. Eur J Mech B Fluids 21(5):495–509

Rist U, Maucher U, Wagner S (1996) Direct numerical simulation of some fundamental problems related to transition in laminar separation bubbles. In: Proceedings of the ECCOMAS computational fluid dynamics conference, pp 319–325

Rist U, Augustin K, Wagner S (2002) Numerical simulation of laminar separation-bubble control. In: Proceedings of the 12th STAB/DGLR symposium. Stuttgart, Germany

Schmidt GS, Mueller TJ (1989) Analysis of low Reynolds number separation bubbles using semiempirical methods. AIAA J 27(8):993–1001

Tani I (1964) Low-speed flows involving bubble separations. Prog Aerosp Sci 5:70–103

Thompson MC, Hourigan K (2005) The shear-layer instability of a circular cylinder wake. Phys Fluids 17:1–4

Timmer WA (2008) Two-dimensional low-Reynolds number wind tunnel results for Airfoil NACA 0018. Wind Eng 32(6):525–537

Watmuff JH (1999) Evolution of a wave packet into vortex loops in a laminar separation bubble. J Fluid Mech 397:119–169

Weibust E, Bertelrud A, Ridder SO (1987) Experimental investigation of laminar separation bubbles and comparison with theory. J Aircr 24(5):291–297

Willmarth WW (1975) Pressure fluctuations beneath turbulent boundary layers. Annu Rev Fluid Mech 7:13–38

Yarusevych S, Boutilier MSH (2011) Vortex shedding of an airfoil at low Reynolds numbers. AIAA J 49(10):2221–2227

Yarusevych S, Sullivan PE, Kawall JG (2005) Airfoil boundary layer separation and control at low Reynolds numbers. Exp Fluids 38(4):545–547

Yarusevych S, Kawall JG, Sullivan PE (2008) Unsteady separated flow characterization on airfoils using time-resolved surface pressure measurements. AIAA J 46(2):508–516

Yarusevych S, Sullivan PE, Kawall JG (2009) On vortex shedding from an airfoil in low-Reynolds-number flows. J Fluid Mech 632:245–271

Zhang W, Hain R, Kähler CJ (2008) Scanning PIV investigation of the laminar separation bubble on a SD7003 airfoil. Exp Fluids 45:725–743